

**Transition from classical to quantum loss of light coherence**

Pierre Lassègues,<sup>1</sup> Mateus Antônio Fernandes Biscassi<sup>1,2</sup>, Martial Morisse,<sup>1</sup> André Cidrim<sup>2,3</sup>,  
 Pablo Gabriel Santos Dias<sup>2</sup>, Hodei Eneriz,<sup>1</sup> Raul Celistrino Teixeira,<sup>2</sup> Robin Kaiser,<sup>1</sup>  
 Romain Bachelard<sup>1,2,\*</sup> and Mathilde Hugbart<sup>1,†</sup>

<sup>1</sup>CNRS, Institut de Physique de Nice, Université Côte d'Azur, 06560 Valbonne, France

<sup>2</sup>Departamento de Física, Universidade Federal de São Carlos, Rodovia Washington Luís, km 235 - SP-310, 13565-905 São Carlos, SP, Brazil

<sup>3</sup>Department of Physics, Stockholm University, 10691 Stockholm, Sweden



(Received 3 October 2022; revised 23 January 2023; accepted 15 September 2023; published 18 October 2023)

Light is a precious tool to probe matter, as it captures microscopic and macroscopic information on the system. However, the measurement will be limited by the coherence of the light, both spatial and temporal, which itself reveals certain properties of the emitters. We here report on the transition from a thermal (classical) to a spontaneous emission (SE) (quantum) mechanism for the loss of light temporal coherence from a macroscopic atomic cloud. The coherence is probed by intensity-intensity correlation measurements realized on the light scattered by the atomic sample, and the transition is explored by tuning the balance between thermal coherence loss and SE via the pump strength. The transition occurs only at low temperatures, which illustrates the potential of cold atom setups to investigate the classical-to-quantum transition in macroscopic systems.

DOI: [10.1103/PhysRevA.108.042214](https://doi.org/10.1103/PhysRevA.108.042214)

**I. INTRODUCTION**

Quantum mechanics has brought a completely new description of a physical system, introducing the possibility of “entanglement” between its different states. However, this diversity in possible states comes at the expense of a dramatic increase in complexity of the phase space, which can be compensated by deriving an effective dynamics for a selected set of degrees of freedom, tracing over the less relevant ones. This loss of information leads to the notion of decoherence [1], and the partial knowledge of the system state allows for an accurate prediction of the dynamics over a finite time only. From a fundamental point of view, decoherence actually questions the notions of measurement, collapse of the wave function [2,3], and hidden variables in quantum mechanics [4].

Let us consider the prototypical example of spontaneous emission (SE) (with rate  $\Gamma$ ) for a quantum emitter: It arises from tracing over the electromagnetic modes in which the particle excitation may be emitted. Yet, while half of the SE rate can be explained by the radiation reaction with a classical approach, the other half was shown to stem from the quantum fluctuations of the modes: “*Die spontane Emission ist somit eine durch die Nullpunktsschwingungen des leeren Raumes erzwungene Emission eines Lichtquants*,” as Weiskopf wrote [5,6]. These zero-point fluctuations do not result from a set of unknown (or “hidden”) variables, as in classical statistical physics when microscopic details are ignored, but rather from Heisenberg’s uncertainty principle [7].

In the case of a quantum emitter, the decoherence mechanism incarnated by SE leaves its mark on the radiated light,

since signatures of the quantum nature of the emitter, such as photon antibunching [8,9] or Rabi oscillations [10,11], are visible on a time scale  $1/\Gamma$ . When moving to many emitters, the nature of the mechanism at the origin of the light coherence loss can be more ambiguous, as one meets the frontier between quantum physics and statistical ensembles. For example, photon antibunching is observed in large systems under specific conditions such as phase matching [12] or confinement of light in fibers [13]; SE then sets the time scale of the light coherence. Differently, the reduction of this coherence time due to the particles’ motion can be understood from a classical perspective: macroscopic information (the velocity distribution) is extracted from the reduction of the light coherence, without the knowledge of the microscopic trajectories, and this effect is at the core of the diffusive wave spectroscopy technique [14–20]. This illustrates the variety of phenomena that compete to set a limit to light coherence.

In this work, we report on the transition from a classical to a quantum mechanism for the loss of coherence in the light scattered by a macroscopic atomic cloud of cold neutral atoms. In the weak drive regime, the atoms scatter light elastically, yet the finite cloud temperature induces a broadening of the spectrum: the coherence loss is here a macroscopic manifestation of the microscopic dynamics (see Fig. 1). Differently, SE dominates the scattering from strongly driven atoms, and the light coherence is then limited by the transition rate  $\Gamma$ . In this regime, the emission of each atom is spectrally broadened [21], and the reduction of coherence results from zero-point fluctuations of the electromagnetic field rather than from unknown microscopic details [22]. Experimentally, we perform intensity-intensity correlation measurements to characterize the (loss of) light coherence: the associated intensity fluctuations are shown to also arise, depending on the regime explored, from either the Doppler effect or SE. Furthermore,

\*romain@ufscar.br

†mathilde.hugbart@inphyni.cnrs.fr

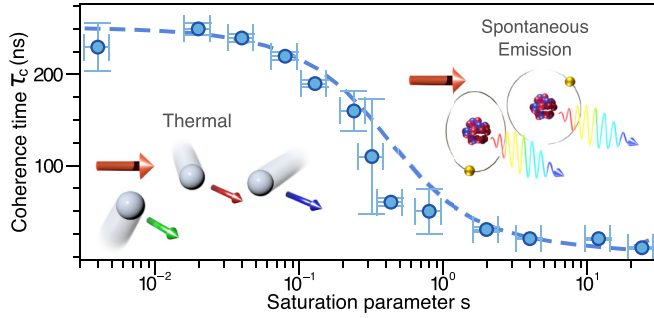


FIG. 1. Coherence time of the light radiated by a macroscopic cloud, as a function of the saturation parameter (dashed: theory; dots: experiment with error bars, see main text). Left inset: For a weak drive on the atoms, the elastically scattered light acquires a frequency shift due to the Doppler effect. The finite temperature of the cloud broadens the light spectrum, setting the coherence time. Right inset: Each of the strongly driven atoms emits a broadened spectrum (Mollow triplet).

we show that a cold sample is necessary for the transition to be observed. Alternatively, we monitor field-field correlations, which confirm that the electric field coherence suffers from the same mechanism as the intensity (Siegert relation), both in the classical and in the quantum regime of coherence loss.

## II. EXPERIMENTAL SETUP

We here detail the setup presented in Fig. 2(a) (see Refs. [23,24] for further details). The scattering medium is produced by loading a magneto-optical trap from a vapor of  $N \approx 10^8$   $^{85}\text{Rb}$  atoms, with a low atomic density  $\rho \approx 0.005/\lambda^3$  ( $\lambda = 2\pi/k$  the optical wavelength). After a 2-ms time of flight, the cloud is illuminated by a flattop intensity laser beam with a frequency  $\omega_L$  locked on the  $|3\rangle \rightarrow |4'\rangle$  hyperfine transition of the D2 line. The beam diameter at the atoms' positions is 14.7 mm, which is much larger than the cloud radius ( $\sim 0.4$  and  $0.8$  mm in the two transverse directions). Hence, the intensity incident on the atoms is uniform (within 10%), with Rabi frequency  $\Omega$ . We use  $\lambda/2$  and  $\lambda/4$  plates to obtain a circularly polarized light, and the intensity is changed to tune the saturation parameter  $s = 2\Omega^2/\Gamma^2$  between 0.004 and 60. To maintain similar heating effects over the different regimes, the duration of the laser pulse, always at resonance, is adjusted to get a constant number of photons scattered per atom of  $\sim 400$ .

The scattered light is collected at  $\theta = 90^\circ$  from the probe beam axis, using a polarization-maintaining (PM) single-mode fiber. The polarization is selected before the fiber with a  $\lambda/2$  plate and a polarization beam splitter (PBS) to maximize the amount of collected photons as well as to adjust the incident polarization along the PM fiber axis. This PM fiber is then connected to a fibered beam splitter (FBS) whose outputs illuminate two single-photon counter detectors (avalanche photodiodes, APDs) connected to a time-to-digital converter (TDC). The latter device allows to time-tag the arrival of each photon. The second input of the fibered beam splitter is used to add a local oscillator (LO) derived from the laser which delivers the probe beam. The LO is frequency shifted by  $\omega_{\text{BN}} = 220$  MHz with an acousto-optical modulator (AOM),

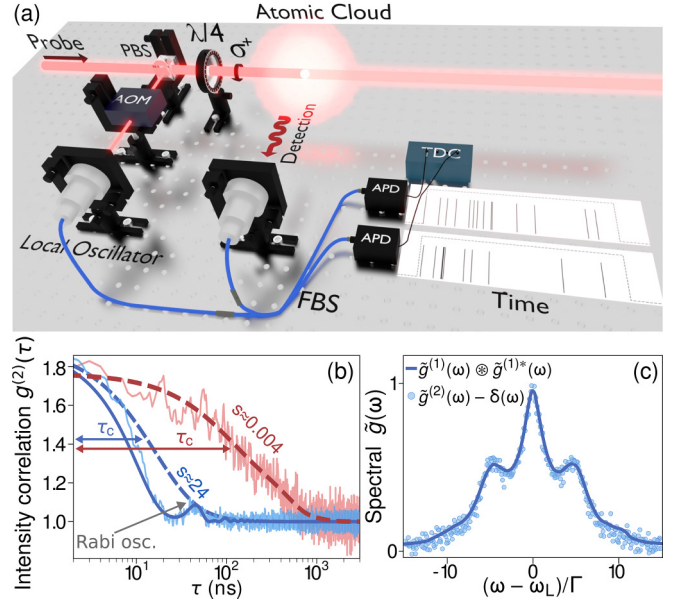


FIG. 2. (a) Schematic setup of the experiment (see main text for details). (b) Temporal evolution of the second-order coherence  $g^{(2)}(\tau)$ , in a low-saturation temperature-dominated regime [ $s = (4.0 \pm 0.8) \times 10^{-3}$ ] and in a high-saturation SE-dominated regime ( $s = 24 \pm 5$ ). Dashed lines: fits of the decay capturing the coherence time; the solid thicker line is a fit containing the (coherent) Rabi oscillation of the saturated regime. (c) Observation of the Siegert relation, which writes  $\bar{g}^{(2)}(\omega) = \delta(\omega) + \bar{g}^{(1)}(\omega) \otimes \bar{g}^{(1)*}(\omega)$  in the frequency space [ $\otimes$  the convolution and  $\delta(\omega)$  the Dirac function], for the large- $s$  regime,  $s \approx 60$ . The elastic component is broadened by the temperature; the spectra are normalized to one.

and its polarization is adjusted before the entrance of the fiber to correspond to the PM fiber axis.

## III. THERMAL COHERENCE LOSS VERSUS SE

Our experimental setup allows us to measure simultaneously the first-order (field-field) and second-order (intensity-intensity) correlation functions of the scattered light [24]:

$$g^{(1)}(\tau) = \frac{\langle \hat{E}^-(t) \hat{E}^+(t + \tau) \rangle}{\langle \hat{E}^-(t) \hat{E}^+(t) \rangle}, \quad (1)$$

$$g^{(2)}(\tau) = \frac{\langle \hat{E}^-(t) \hat{E}^-(t + \tau) \hat{E}^+(t + \tau) \hat{E}^+(t) \rangle}{\langle \hat{E}^-(t) \hat{E}^+(t) \rangle^2}. \quad (2)$$

$\hat{E}^+$  refers to the positive frequency component of  $\hat{E}$  of the electric field in the measured mode,  $\langle \cdot \rangle$  either to the average over time or to the expectation value [25], and we here consider the steady-state limit,  $t \rightarrow \infty$ . In all cases, we also average over configurations.

Two examples of  $g^{(2)}(\tau)$  correlation functions taken from the experiment are presented in Fig. 2(b). Let us now discuss how the coherence time, which is the typical time scale over which the  $g^{(2)}(\tau)$  falls to unity, is extracted. Two regimes must be distinguished: First, for a weak pump ( $s \ll 1$ ), most light is scattered elastically by each atom in its own (moving) frame. In the laboratory frame, this atomic motion translates into a change in frequency of the light (Doppler effect), and

the interference between the fields scattered by the disordered ensemble of moving atoms leads to a Doppler-broadened spectrum with coherence time  $\tau_c^T \propto 1/\sqrt{T}$  [see red curve in Fig. 2(b)], with  $T$  the temperature. In this limit case of  $s \ll 1$ , the experimental  $g^{(2)}(\tau)$  curve can be fitted by a decaying exponential, and the coherence time corresponds to its half-width at half-maximum (HWHM). The temperature-induced  $\tau_c^T$  is extrapolated for  $s = 0$  from measurements at several low- $s$  values, and the value obtained,  $\tau_c^T \approx 260$  ns, corresponds to a temperature of about 200  $\mu\text{K}$  and a cloud with an optical depth of 6 [20], see Appendix A. This statistical analysis is a purely classical mechanism of coherence loss.

In the second regime, the coherence loss is based on the quantum randomness of SE, and it is reached using a strong resonant pump ( $s \gg 1$ ). Each atom then presents a spectrally broadened fluorescence, the so-called Mollow triplet [21,26], which is characterized by a peak at resonance and two sidebands shifted by  $\pm\Omega$  from the carrier, with  $\Omega$  the pump Rabi frequency. The beating between these peaks of inelastic scattering is manifested as Rabi oscillations in the  $g^{(2)}(\tau)$ , whereas the widths of the peaks ( $\Delta\omega \approx \Gamma$ ) set the coherence time of this spontaneously emitted light, see Fig. 2(b). In the  $s \gg 1$  limit, the  $g^{(2)}(\tau)$  can be fitted by the square of a sum of an exponential (for the peaks of the Mollow triplet) and a cosine modulated by a decaying exponential (for the beating between sidebands and the carrier). The coherence time is then extracted as the HWHM of the nonoscillating part of the fit, providing the value  $\tau_c^{\text{SE}} \approx 16$  ns (see Appendix A 2). This broadening mechanism does not rely on the microscopic state of the system (and macroscopically captured by temperature, for example) or any “hidden variable,” but rather on zero-point fluctuations [22].

In our experiment, the transition between the classical and quantum regimes occurs when the ratio of spontaneously emitted to elastically scattered power is inverted. This ratio here corresponds to the saturation parameter  $s$  [8,21], tuned via the pump strength  $\Omega$ . In Fig. 1, we present the evolution of the coherence time of the light when crossing from the classical to the quantum regime of coherence loss. For arbitrary values of  $s$ , the coherence time is then extracted as the HWHM of the nonoscillating part of the fit of the corresponding  $g^{(2)}(\tau)$  by the square of a weighted sum of the thermal and Mollow fitting functions, and it is the method used to compute  $\tau_c$  throughout this work. The slightly larger coherence time observed for intermediate  $s$  in the experiment (see Fig. 1), as compared to the theoretical prediction, can be attributed to the attenuation of the beam during its propagation in the cloud, which results in an increase of the relative contribution of elastic scattering. The overall agreement between the experimental and theoretical curves shows that the proposed picture of  $N \gg 1$  independent atoms captures well the underlying physical mechanisms of coherence loss for the light.

This classical-to-quantum transition is observed for low temperatures such that the thermal coherence time  $\tau_c^T$ , of the order of  $\sqrt{M/k_B T}/k$  [20] (with  $M$  the atomic mass,  $k_B$  the Boltzmann constant, and  $k$  the light wave vector), is much larger than the coherence time of SE  $\tau_c^{\text{SE}}$ , of the order of  $\Gamma^{-1}$ . In this regime, the Doppler broadening does not affect substantially the Mollow triplet, as is the case in our experiment. However, for temperatures larger than  $T_{\text{crit}} = (\Gamma/k)^2 M/k_B$

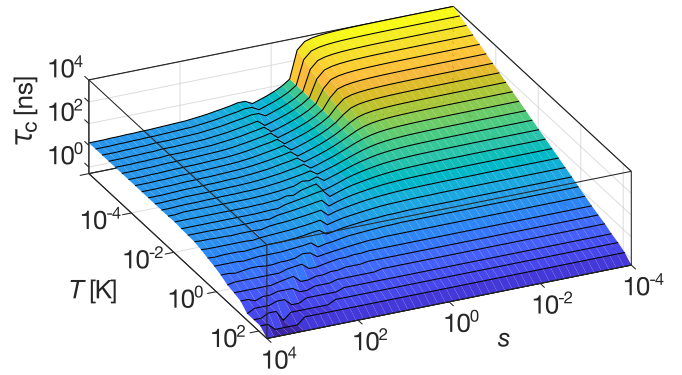


FIG. 3. Theoretical coherence time of the light scattered by the atomic cloud, at an angle  $90^\circ$  from the probe beam axis, as a function of the cloud temperature  $T$  and the saturation parameter  $s$  of the probe. The small oscillations close to the transition originate from the fitting procedure when the fitting model for the Doppler broadening and for the SE are competing with comparable weights to fit the  $g^{(2)}$  curves.

(0.1 K for Rubidium atoms), the transition is attenuated since the Doppler broadening starts to affect substantially the Mollow triplet ( $s \gg 1$ ) of each atom. Then, the thermal motion competes with the triplet as a mechanism for the loss of light coherence. This dependence of the transition on the temperature is illustrated in Fig. 3, and it demonstrates the necessity of working with a cold platform to observe a clear transition between the Doppler broadening and SE regimes of light coherence loss.

#### IV. ORIGIN OF THE FLUCTUATIONS

The finite coherence time reflects the fluctuations of the intensity over time, which can have different origins. Elastically scattered light is usually treated as a continuously radiated field, whose fluctuations result from the emitters’ motion, whereas SE can be thought of as the emission of quanta of light. Although the two pictures of continuous versus discrete detection events can be reconciled [25,27], let us now discuss how the fluctuations observed in each regime nevertheless depend on the underlying physical mechanism.

Let us first consider motionless particles scattering light elastically. One may expect the light emitted by the cloud to inherit the same statistics of the pump,  $g^{(2)}(0) = 1$  for a laser. Yet this classical picture presents a loophole, as one already perceives from the test case of a pair of two-level atoms. Under a resonant drive with wave vector  $\mathbf{k}_L$ , two remote (noninteracting) two-level atoms at positions  $\mathbf{r}_{1,2}$  exhibit a second-order correlation function at zero delay which satisfies [28] (see also Appendix B)

$$g^{(2)}(0) = \frac{(s+1)^2}{(s+1 + \cos[(k\hat{n} - \mathbf{k}_L) \cdot (\mathbf{r}_2 - \mathbf{r}_1)])^2}, \quad (3)$$

in the far field and in the steady state, and with  $\hat{n}$  the direction of observation. The cosine is an interference term that produces an angular dependence for the  $g^{(2)}(0)$ . For  $N = 2$  this term is present in the intensity  $\langle \hat{E}^- \hat{E}^+ \rangle$ , yet absent from the two-photon term  $G^{(2)} = \langle \hat{E}^- \hat{E}^- \hat{E}^+ \hat{E}^+ \rangle$ , and it leads to the spatial modulation of the light statistics reported in pairs of

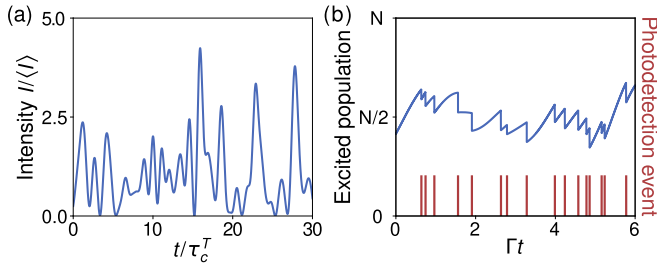


FIG. 4. (a) Evolution of the emitted intensity from a cloud of moving classical dipoles with positions  $\mathbf{r}_j(t)$ , where the Doppler effect combines with interference to provide temporal fluctuations:  $I \propto |\sum_j \exp[i(\mathbf{k}_L - k\hat{n}) \cdot \mathbf{r}_j(t)]|^2$ , with  $\hat{n}$  the direction of observation, and  $\langle \dot{r}_j^2 \rangle = k_B T/M$ . (b) Stochastic evolution of the excited population of an ensemble of  $N$  atoms driven by a strong pump, in the steady state, obtained from exact simulations of strongly driven two-level atoms [32] (with  $N = 10$  and  $s = 8$ ). The quantum jumps toward a lower population state correspond to the emission of a photon (photodetection events in red).

trapped ions [29]. This result is at odds with a linear optics approach mentioned above, where motionless scatterers emit a constant electric field, corresponding to  $g^{(2)}(0) = 1$  (coherent light). The flaw in the latter approach is that the emission of two photons, as measured by the  $g^{(2)}$  function, cannot be described classically. Note that this feature is absent from field-field correlations (1), which is equal to one at zero delay by definition: the  $g^{(1)}$  function does not address photons, but only fields.

In particular, the angles such that  $(k\hat{n} - \mathbf{k}_L) \cdot (\mathbf{r}_2 - \mathbf{r}_1) = \pi \pmod{2\pi}$  correspond to destructive interference, at which the emission computed from the optical coherences of the two-level atoms (that is, the elastically scattered component) cancels. In those particular directions, only a contribution from the doubly excited state remains and one obtains  $g^{(2)}(0) = (s+1)^2/s^2$ , which diverges in the  $s \rightarrow 0$  limit [28], even in the large  $N$  case (see Appendix B). Yet far from any divergence, the intensity correlations observed in the experiment lead to  $g^{(2)}(0) \approx 2$  in the low- $s$  regime, expected from chaotic light. This finite value is due to the finite temperature of the cloud, along with the finite time necessary to evaluate the  $g^{(2)}(\tau)$ , see Appendix A. Indeed, the atomic motion results in spatiotemporal fluctuations of the speckle field. Thus, the measurement of the  $g^{(2)}$  over a time scale much larger than the coherence time of the speckle provides a finite *averaged* value of the intensity, and thus a finite intensity variance  $g^{(2)}(0)$ . In other words, in the classical regime, the notation  $\langle \cdot \rangle$  refers to a statistical average on the thermal probability distribution of atomic positions and velocities. In our experiment, the average is realized over the duration of the experiment ( $>20 \mu\text{s}$ ), much larger than the coherence time  $\tau_c^T$  of the speckle grain, and over different clouds, which explains why the value  $g^{(2)}(0) = 2$  is observed. In this low- $s$  regime, a description of the scatterers as moving classical dipoles leads to the same conclusion [30,31]. An example of this classical description is illustrated in Fig. 4(a), where the intensity emitted in a given direction by classical dipoles with ballistic trajectories is shown. The value  $g^{(2)}(0) = 2$  and the coherence time  $\tau_c^T \approx 260$  ns obtained from this approach are the same as the ones observed in the

experiment, which supports the classical origin of coherence loss in this regime.

Differently, SE gives rise to intensity fluctuations even in the absence of any motion. The random nature of the photon emission in this regime is best understood by adopting the quantum jump approach [33]. While the atomic ensemble undergoes coherent Rabi oscillations under the action of the drive, it also stochastically decays toward a lower population state when a photon is spontaneously emitted. This process is illustrated in Fig. 4(b), where the total excited population of a cloud of  $N$  atoms is presented for a given realization (or “trajectory”). At each decay event, a photodetection occurs (see red lines). In the experiment [inset in Fig. 2(a)], the correlation between the detection event times of the two detectors is computed, before a binning over a time window much smaller than the coherence time of the light is applied. This experimental protocol effectively measures the expectation value, with a temporal average, of the operators involved in the definition of  $g^{(2)}(\tau)$ , see Eq. (2), and it provides the continuous curves presented in Fig. 2(b).

In the experiment [APDs’ signal in Fig. 2(a)], the correlation between the detection events of the two detectors is computed, before a binning over a time window much smaller than the coherence time of the light is applied. This experimental protocol effectively measures the expectation value, with a temporal average, of the operators involved in the definition of  $g^{(2)}(\tau)$ , and it provides the continuous curves presented in Fig. 2(b).

The amplitude of the fluctuations that we observe,  $g^{(2)}(0) \approx 2$ , is consistent with the value for chaotic light. A common picture for a gas of particles is when each emitter emits a field with a given phase, yet with a mechanism that randomizes this phase [25]. In our experiment, the temperature provides this dephasing mechanism for the elastic component of the scattering, which dominates at low  $s$ . Nonetheless, the calculation of  $g^{(2)}(0)$  shows that the classical and quantum regimes studied here are qualitatively different (see Appendix B). In the quantum regime ( $s \gg 1$ ), the absence of a well-defined phase for the field from each two-level emitter is a result of the SE of the photons, and the atomic motion, or other classical dephasing mechanisms such as collisions, are unnecessary to explain the fluctuations in the intensity of spontaneously emitted light. An additional signature that the emission in the large- $s$  regime comes from quantum emitters is the Rabi oscillation observed in the  $g^{(2)}(\tau)$  of Fig. 2(b), which results from the coherent dynamics between the two levels of the atoms (with a circularly polarized large- $s$  pump, the atoms are driven to an extreme Zeeman sublevel, from which a two-level transition only is explored).

## V. FIELD FLUCTUATIONS AND SIEGERT RELATION

Elastically scattered light has a well-defined phase, which is determined by the incident laser and the trajectories of the atoms. For SE, the broadened fluorescence spectrum of even single atoms, along with the absence of a phase operator [34,35], prevent a direct analogy. Nevertheless, the electric field from SE possesses a temporal coherence, which is captured by field-field correlations, see Eq. (1). In our setup,

it is obtained from the homodyne measurements described previously.

In Fig. 2(c), we present simultaneous measurements of the  $g^{(1)}$  and the  $g^{(2)}$  functions, in the strong drive regime ( $s \approx 60$ ). The excellent match between intensity-intensity correlations and the square modulus of field-field correlations corresponds to the Siegert relation,  $g^{(2)}(\tau) = 1 + |g^{(1)}(\tau)|^2$ , which establishes an equivalence between the (loss of) coherence for the field and the intensity [36].

The textbook derivation of the Siegert relation [25] relies on three conditions: a large number of scatterers, the absence of correlations between the emitters (here supported by the negligible interactions), and a zero average electric field  $\langle \hat{E}_j \rangle$  for each emitter  $j$ . The latter condition is provided, for elastic scattering, by thermal motion [25]. For SE, the absence of coherence between ground and excited states of each atom  $j$  guarantees  $\langle \hat{E}_j^- \rangle = 0$  (despite  $\langle \hat{E}_j^- \hat{E}_j^+ \rangle \neq 0$ ), even in the absence of motion. Yet, even the sum of the two kinds of emission, as encountered in the intermediate  $s$  regime, satisfies the Siegert relation V. The reason is that elastically scattered and spontaneously emitted light are uncorrelated fields, with independent mechanisms to provide the zero average of the field: Thermal motion relies on the external degrees of freedom of the emitters, whereas SE stems from zero-point fluctuations.

## VI. CONCLUSIONS

We have investigated the transition from thermal to SE for loss of light coherence in a macroscopic cold atomic cloud using intensity-intensity correlation measurements. This transition is monitored by tuning the pump power, which controls the ratio between elastic scattering (subjected to thermal broadening) and SE. We also demonstrated that a low temperature is required to observe the transition, which highlights the potential of cold atomic samples to explore the frontier between statistical physics and quantum effects in large systems.

The transition occurs in the absence of interactions between the emitters. An open question is how collective effects arising, for example, from dipole-dipole interactions (super- and subradiance) may leave a mark on light coherence. The original configuration envisioned for superradiance was the decay cascade from a fully excited state to the ground state of a many-atom cloud [37], which is intrinsically an out-of-equilibrium dynamics. Steady-state signatures of collective effects for atoms in free space remain to be explored, which could lead to new phase transitions [38–40]. In this context, it is worth mentioning a recent report of steady-state superradiance in intensity correlations measurements in a four-wave mixing experiment [41].

## ACKNOWLEDGMENTS

The authors acknowledge funding from the French National Research Agency (Projects No. PACE-IN ANR19-QUAN-003-01 and No. QuaCor ANR19-CE47-0014-01). M.A.F.B., A.C., and R.B. benefited from Grants from the São Paulo Research Foundation (FAPESP, Grants No. 2021/02673-9, No. 2017/09390-7, No. 2018/15554-5, No. 2019/13143-0, No. 2022/06449-9, and No. 2023/07463-8) and from the National Council for Scientific and Technological Development (CNPq, Grants No. 409946/2018-4 and

No. 313886/2020-2). R.K., R.B., and M.H. received support from the project STIC-AmSud (No. Ph879-17/CAPES 88887.521971/2020-00). We also acknowledge the financial support of the Doebelin Federation, and R.K. received support from the European project ANDLICA, ERC Advanced Grant Agreement No. 832219. M.H. has been supported by the European Unions Horizon 2020 research and innovation programme in the framework of the Marie Skłodowska-Curie HALT project (Grant Agreement No. 823937). A.C. and R.B. acknowledge support by the CAPES-STINT collaboration (Grant No. 88887.649265/2021-00).

## APPENDIX A: THEORETICAL APPROACH FOR THE LIGHT COHERENCE TIME

### 1. Modeling

We assume that the atomic cloud has a Maxwell-Boltzmann distribution of velocities (temperature  $T$ ) and, at first, a low optical thickness so that multiple scattering and collective effects can be neglected. The probe is a monochromatic wave with a frequency set to the atomic resonance. The scattered spectrum is computed for the different atomic velocity classes, between  $\mathbf{v}$ ,  $\mathbf{v} + d\mathbf{v}$ . For each velocity class, this spectrum is the sum of an elastic and an inelastic component. The elastic one corresponds to a Dirac function, yet Doppler shifted from the probe frequency. As for the inelastic part, we first compute the Mollow spectrum for the saturation parameter  $s$ , taking into account the detuning of the probe beam by moving to the atom frame, before converting back this spectrum to the observation frame. Finally, we integrate the sum of the elastic and inelastic components over the distribution of atomic velocities to obtain the total scattered spectrum, related to the Fourier transform of the field-field correlation function  $g^{(1)}(\tau)$ . Assuming the Siegert relation, one computes the  $g^{(2)}(\tau)$  function to extract its temporal coherence  $\tau_c$ , as presented in Fig. 1. For the theory curve in Fig. 1, the effective temperature  $T_{\text{eff}} = 1.7$  mK is used, which accounts for the multiple scattering in a cloud with optical thickness  $b \approx 6$  in the low- $s$  regime, as discussed in Ref. [20]. Multiple scattering by moving atoms indeed results in a reduction of the thermal coherence time, as compared to the single scattering regime. Because our analysis relies on a single scattering assumption (independent scatterers hypothesis), we resort to this effective temperature to describe the loss of coherence by thermal motion. This choice is motivated by the challenge of dealing simultaneously with multiple and inelastic scattering in the moderate- $s$  regime, which is beyond the scope of our work. In summary, this reduced coherence time can be taken into account by either multiple scattering and the “real temperature” of the cloud or, alternatively, using a simpler single parameter with a larger “effective temperature,” which in our case corresponds to an effective temperature of 1.7 mK (instead of the “real temperature” of 200  $\mu$ K).

### 2. Fitting protocol

To extract the temporal coherence from the  $g^{(2)}(\tau)$  functions, either modeled theoretically or obtained experimentally, we first assume that these curves are the sum of a contribution from (1) the thermal motion and (2) the temporal counterpart

of the Mollow triplet for the inelastic component. The former corresponds to a Gaussian in time for the single scattering regime (theoretical curves of Fig. 3); for the experimental data in Fig. 1, we have used a decaying exponential in time to account for the presence of multiple scattering, which results from the Lorentzian shape of the elastic component in frequency space [20]. The relative weight of each component is determined by taking into account the saturation parameter [8]. This leads to a  $g^{(2)}(\tau)$  function of the form

$$g^{(2)}(\tau) - 1 = \left| Af_{\text{el}}(\tau) + (1 - A) \times \left( \frac{1}{2} e^{-|\tau|/\tau_c^{\text{SE}}} + \frac{1}{4} (e^{i\Omega_\Gamma B\tau} + e^{-i\Omega_\Gamma C\tau}) e^{-|\tau|/\tau_s} \right) \right|^2, \quad (\text{A1})$$

with the generalized Rabi frequency  $\Omega_\Gamma^2 = \Omega^2 - (\frac{\Gamma}{4})^2$ , the Rabi frequency  $\Omega = \Gamma\sqrt{s/2}$  [8], and  $f_{\text{el}}(\tau) = e^{-|\tau|/\tau_{\text{el}}}$  or  $e^{-\tau^2/\tau_{\text{el}}^2}$  the elastic scattering component. Our experimental intensity correlation functions are fitted by this formula, with  $A, B, C, \tau_{\text{el}}, \tau_c^{\text{SE}}$ , and  $\tau_s$  as free parameters [solid thicker line in Fig. 2(b)] and  $\Omega$  and  $s$  being obtained from the direct measurement of the probe intensity. As mentioned previously, the coherence time is then defined as the HWHM of the nonoscillating part of the former fit (that is, the complex exponentials in the fitting formula are set to one for  $\Omega_\Gamma$  real). Since the theoretical  $g^{(2)}(\tau)$  functions do not present noise, we directly fit the nonoscillating part on the monotonous part of the curve computed, which provides  $\tau_c^{\text{SE}} \approx 16$  ns. Note that the decay constants  $\tau_c^{\text{SE}}$  and  $\tau_s$  are treated as two independent fitting parameters, to account for the fact that the carrier and the Mollow sidebands suffer from several broadening mechanisms (fluctuations in the probe profile, Doppler broadening).

## APPENDIX B: SECOND-ORDER CORRELATION FUNCTION $g^{(2)}(0)$ FOR $N$ NONINTERACTING ATOMS

We derive here the analytical expression for the second-order correlation function at zero delay  $g^{(2)}(0)$  for an ensemble of  $N$  two-level noninteracting atoms. The detected electric field is assumed to be measured in the far-field and along a direction  $\hat{n}$ , so it reads

$$\hat{E}^+ = E_0 \sum_{a=1}^N e^{-ik\hat{n}\cdot\mathbf{r}_a} \hat{\sigma}_a^-, \quad (\text{B1})$$

with  $\mathbf{r}_a$  the position vector of atom  $a$ ,  $\hat{\sigma}_a^\mp$  the two-level lowering or raising spin operation, and  $E_0$  a normalization prefactor. Without loss of generality, we hereafter set  $E_0 = 1$ , resulting in a normalized electric field intensity that peaks at unity for a single atom. We also assume that the atomic cloud is dilute, thus interaction between the atoms can be disregarded and the steady state of the system is separable. We can then write the state of the system as a direct product as follows:

$$\hat{\rho} = \bigotimes_{a=1}^N \hat{\rho}_a, \quad (\text{B2})$$

where  $\hat{\rho}_a$  is the single-particle density matrix.

## 1. Scattered field intensity

Let us first calculate the intensity of the field scattered by the atomic ensemble, which reads

$$I = \langle \hat{E}^- \hat{E}^+ \rangle = \sum_{ab} \text{Tr} e^{ik\hat{n}\cdot\mathbf{r}_a} \hat{\sigma}_a^+ e^{-ik\hat{n}\cdot\mathbf{r}_b} \hat{\sigma}_b^- \hat{\rho} \\ = \sum_a \text{Tr} \hat{\sigma}_a^+ \hat{\sigma}_a^- \hat{\rho} + \sum'_{ab} \text{Tr} e^{ik\hat{n}\cdot\mathbf{r}_a} \hat{\sigma}_a^+ e^{-ik\hat{n}\cdot\mathbf{r}_b} \hat{\sigma}_b^- \hat{\rho}, \quad (\text{B3})$$

where we have introduced the notation  $\sum'_{a,b,\dots,n} \equiv \sum_a \sum_{b \neq a} \dots \sum_{n \neq a,b,\dots,n-1}$ .

Using now the separability of the atomic state as in Eq. (B2) and conveniently introducing the excited population

$$n_a \equiv \text{Tr} \hat{\sigma}_a^+ \hat{\sigma}_a^- \hat{\rho}_a \quad (\text{B4})$$

and the coherence

$$\beta_a \equiv e^{-ik\hat{n}\cdot\mathbf{r}_a} \text{Tr} \hat{\sigma}_a^- \hat{\rho}_a \Rightarrow \beta_a^* \equiv e^{ik\hat{n}\cdot\mathbf{r}_a} \text{Tr} \hat{\sigma}_a^+ \hat{\rho}_a, \quad (\text{B5})$$

we can rewrite Eq. (B3) as

$$I = \sum_a n_a + \sum'_{ab} \beta_a^* \beta_b, \\ = \sum_a n_a + \left| \sum_a \beta_a \right|^2 - \sum_a |\beta_a|^2. \quad (\text{B6})$$

## 2. Unnormalized second-order correlation function

Similarly, following the separability of the atomic state, the second-order correlation reads

$$G^{(2)}(0) = \langle \hat{E}^- \hat{E}^- \hat{E}^+ \hat{E}^+ \rangle \\ = 2 \sum'_{ab} \text{Tr} \hat{\sigma}_a^+ \hat{\sigma}_a^- \hat{\rho}_a \text{Tr} \hat{\sigma}_b^+ \hat{\sigma}_b^- \hat{\rho}_b \\ + 4 \sum'_{abc} \text{Tr} \hat{\sigma}_a^+ \hat{\sigma}_a^- \hat{\rho}_a \text{Tr} e^{ik\hat{n}\cdot\mathbf{r}_b} \hat{\sigma}_b^+ \hat{\rho}_b \\ \times \text{Tr} e^{-ik\hat{n}\cdot\mathbf{r}_c} \hat{\sigma}_c^- \hat{\rho}_c \\ + \sum'_{abcd} \text{Tr} e^{ik\hat{n}\cdot\mathbf{r}_a} \hat{\sigma}_a^+ \hat{\rho}_a \text{Tr} e^{ik\hat{n}\cdot\mathbf{r}_b} \hat{\sigma}_b^+ \hat{\rho}_b \\ \times \text{Tr} e^{-ik\hat{n}\cdot\mathbf{r}_c} \hat{\sigma}_c^- \hat{\rho}_c \text{Tr} e^{-ik\hat{n}\cdot\mathbf{r}_d} \hat{\sigma}_d^- \hat{\rho}_d. \quad (\text{B7})$$

Using the definitions in Eqs. (B4) and (B5), we are left with

$$G^{(2)}(0) = 2 \sum'_{ab} n_a n_b + 4 \sum'_{abc} n_a \beta_b^* \beta_c + \sum'_{abcd} \beta_a^* \beta_b^* \beta_c \beta_d. \quad (\text{B8})$$

Reorganizing the expression using sums without index exclusion, one can expand the expression above as

$$G^{(2)}(0) = 2 \left( \sum_a n_a \right)^2 - 2 \sum_a n_a^2 \\ + 4 \left( \sum_a n_a \right) \left( \left| \sum_b \beta_b \right|^2 - \sum_b |\beta_b|^2 \right) \\ - 8 \text{Re} \left\{ \left( \sum_a n_a \beta_a^* \right) \left( \sum_b \beta_b \right) \right\} + 8 \sum_a n_a |\beta_a|^2$$

$$\begin{aligned}
 & + \left| \sum_a \beta_a \right|^4 - 6 \sum_a |\beta_a|^4 - 4 \left| \sum_a \beta_a \right|^2 \left( \sum_b |\beta_b|^2 \right) \\
 & + 8 \operatorname{Re} \left\{ \left( \sum_a \beta_a \right) \left( \sum_b |\beta_b|^2 \beta_b^* \right) \right\} + 2 \left( \sum_a |\beta_a|^2 \right)^2 \\
 & - 2 \operatorname{Re} \left\{ \left( \sum_a \beta_a \right)^2 \left( \sum_b \beta_b^* \right)^2 \right\} + \left| \sum_a \beta_a^2 \right|^2.
 \end{aligned} \tag{B9}$$

### 3. Separable steady state as a function of the saturation parameter

Considering a laser with wave vector  $\mathbf{k}_L$  driving a two-level atom on its resonance at a Rabi frequency  $\Omega$ , the single-atom density matrix in the steady state is given by

$$\hat{\rho}_a = \rho_{ee}^{(a)} |e\rangle\langle e| + \rho_{eg}^{(a)} |e\rangle\langle g| + \rho_{ge}^{(a)} |g\rangle\langle e| + \rho_{gg}^{(a)} |g\rangle\langle g|, \tag{B10}$$

with

$$\begin{aligned}
 \rho_{ge}^{(a)} &= \left( \rho_{eg}^{(a)} \right)^* = -i \frac{e^{(-i\mathbf{k}_L)\mathbf{r}_a}}{1+s} \sqrt{\frac{s}{2}}, \\
 \rho_{ee}^{(a)} &= \frac{s}{2(1+s)}, \\
 \rho_{gg}^{(a)} &= \frac{2+s}{2(1+s)},
 \end{aligned} \tag{B11}$$

where  $s \equiv 2\Omega^2/(\Gamma^2 + 4\Delta^2)$  is the saturation parameter, which on resonance ( $\Delta = 0$ ) reduces to the ratio  $s = 2\Omega^2/\Gamma^2 = P_{SE}/P_{EL}$ , as discussed in the main text.

Substituting the elements of the single-particle density matrix in the definition of  $g^{(2)}(0) = G^{(2)}(0)/I^2$ , one is left with

$$\begin{aligned}
 g^{(2)}(0) &= \frac{1}{(Ns + |\Phi_1|^2)^2} (2Ns[2 + (N-1)s] \\
 &+ 4s(N-2)|\Phi_1|^2 + |\Phi_1^2 - \Phi_2|^2),
 \end{aligned} \tag{B12}$$

where we have defined

$$\begin{aligned}
 \Phi_1 &= \sum_a e^{i(k\hat{n} - \mathbf{k}_L)\cdot\mathbf{r}_a}, \\
 \Phi_2 &= \sum_a e^{i2(k\hat{n} - \mathbf{k}_L)\cdot\mathbf{r}_a}.
 \end{aligned} \tag{B13}$$

For  $s \rightarrow \infty$ , one recovers the formula  $g^{(2)}(0) = 2(1 - 1/N)$  [42], which goes to 2 in the large  $N$  limit. In the limit  $s \rightarrow 0$  where elastic scattering dominates, the destructive interference condition  $\Phi_1 = 0$  leads to a  $g^{(2)}(0)$  scaling as  $(|\Phi_2|/sN)^2$ , which diverges for  $s \rightarrow 0$  at fixed  $N$ . In this regime, thermal motion or another dephasing mechanism is necessary to recover the value  $g^{(2)}(0) = 2$  of chaotic light.

### APPENDIX C: SIEGERT RELATION FOR TWO INDEPENDENT FIELDS

Here we show in a condensed manner that the sum of two fields, each satisfying the Siegert relation and the associated

conditions described in the main text, also satisfies the relation, provided that the fields are uncorrelated. The derivation is provided for two arbitrary electric fields  $\hat{E}_e^+$  and  $\hat{E}_i^+$  corresponding, for example, to the elastically and inelastically (that is, spontaneously emitted) electric fields of the main text. The total electric field is  $\hat{E}^+ = \hat{E}_e^+ + \hat{E}_i^+$ , and it presents the following second-order correlation function in the steady state:

$$\begin{aligned}
 G^{(2)}(\tau) &= \langle [\hat{E}_e^-(t) + \hat{E}_i^-(t)][\hat{E}_e^-(t+\tau) + \hat{E}_i^-(t+\tau)] \\
 &\quad \times [\hat{E}_e^+(t+\tau) + \hat{E}_i^+(t+\tau)][\hat{E}_e^+(t) + \hat{E}_i^+(t)] \rangle.
 \end{aligned} \tag{C1}$$

Both elastic and inelastic terms of the electric field have a zero average:  $\langle \hat{E}_{e,i} \rangle = 0$ , so their sum as well:  $\langle \hat{E} \rangle = 0$ . Furthermore, the absence of correlation between the fields means that the contributions from the elastic and inelastic terms can be factorized in the above expression of  $G^{(2)}$ , which in turn leads to the cancellation of several terms:

$$\begin{aligned}
 G^{(2)}(\tau) &= \langle \hat{E}_e^-(t) \hat{E}_e^-(t+\tau) \hat{E}_e^+(t+\tau) \hat{E}_e^+(t) \rangle \\
 &\quad + \langle \hat{E}_i^-(t) \hat{E}_i^-(t+\tau) \hat{E}_i^+(t+\tau) \hat{E}_i^+(t) \rangle \\
 &\quad + 2 \langle \hat{E}_e^-(t) \hat{E}_e^+(t) \rangle \langle \hat{E}_i^-(t) \hat{E}_i^+(t) \rangle \\
 &\quad + 2 \operatorname{Re}[\langle \hat{E}_e^-(t+\tau) \hat{E}_e^+(t) \rangle \langle \hat{E}_i^-(t) \hat{E}_i^+(t+\tau) \rangle].
 \end{aligned} \tag{C2}$$

Considering now that each scatterer presents the same single-particle correlation functions  $G_{e,i}^{s(1)}(\tau)$  and contributes equally to the total field, then the single emitter correlation function of the field writes  $G^{s(1)}(\tau) = G_e^{s(1)}(\tau) + G_i^{s(1)}(\tau)$ , where we have used that the fields are uncorrelated and have zero average. The correlation function of the total field is then equal to  $\langle \hat{E}^-(t) \hat{E}^-(t+\tau) \rangle = N G^{s(1)}(\tau)$ , with  $N$  the number of scatterers. Calling  $G_{e,i}^{(2)}(\tau)$  the non-normalized second-order correlation function of the total elastic or inelastic terms, respectively, we obtain

$$\begin{aligned}
 G^{(2)}(\tau) &= G_e^{(2)}(\tau) + G_i^{(2)}(\tau) + 2N^2 G_e^{s(1)}(0) G_i^{s(1)}(0) \\
 &\quad + 2N^2 \operatorname{Re}[G_e^{s(1)}(\tau) G_i^{s(1)*}(\tau)].
 \end{aligned} \tag{C3}$$

Assuming that the spectrum emitted by a single atom is symmetric, its Fourier transform  $G_{e,i}^{s(1)}(\tau)$  is real. We also assumed that both the elastic and inelastic fields satisfy the Siegert relation, so (C3) can be rewritten as

$$\begin{aligned}
 G^{(2)}(\tau) &= N^2 \left( [G_e^{s(1)}(0)]^2 + [G_e^{s(1)}(\tau)]^2 \right) \\
 &\quad + N^2 \left( [G_i^{s(1)}(0)]^2 + [G_i^{s(1)}(\tau)]^2 \right) \\
 &\quad + 2N^2 G_e^{s(1)}(0) G_i^{s(1)}(0) + 2N^2 G_e^{s(1)}(\tau) G_i^{s(1)}(\tau).
 \end{aligned} \tag{C4}$$

This can be simplified to

$$\begin{aligned}
 g^{(2)}(\tau) &= \frac{[G_e^{s(1)}(0) + G_i^{s(1)}(0)]^2 + [G_e^{s(1)}(\tau) + G_i^{s(1)}(\tau)]^2}{[G_e^{s(1)}(0) + G_i^{s(1)}(0)]^2} \\
 &= 1 + |g^{(1)}(\tau)|^2.
 \end{aligned} \tag{C5}$$

Thus, the sum of two uncorrelated Siegert-satisfying fields still satisfies the Siegert relation. For our particu-

lar system, it implies that in the intermediate saturation regime, where both elastic and inelastic scattering occur,

the Siegert relation is verified for a large number of scatterers.

- 
- [1] H.-P. Breuer and F. Petruccione, *The Theory of Open Quantum Systems* (Oxford University Press, 2007).
- [2] W. H. Zurek, Decoherence, einselection, and the quantum origins of the classical, *Rev. Mod. Phys.* **75**, 715 (2003).
- [3] D. Wallace, Decoherence and its role in the modern measurement problem, *Philos. Trans. R. Soc. A* **370**, 4576 (2012).
- [4] H. D. Zeh, On the interpretation of measurement in quantum theory, *Found. Phys.* **1**, 69 (1970).
- [5] V. Weisskopf, Probleme der neueren quantentheorie des elektrons, *Naturwissenschaften* **23**, 631 (1935).
- [6] It can be translated as “SE is thus a stimulated emission of one quantum of light caused by the zero point fluctuations of the vacuum.”
- [7] R. A. Newing, Uncertainty principle and the zero-point energy of the harmonic oscillator, *Nature (London)* **136**, 395 (1935).
- [8] D. A. Steck, Quantum and atom optics, available online at <http://steck.us/teaching> (revision 0.14, 23 August 2023).
- [9] M. Dagenais and L. Mandel, Investigation of two-time correlations in photon emissions from a single atom, *Phys. Rev. A* **18**, 2217 (1978).
- [10] B. W. Shore and P. L. Knight, The Jaynes-Cummings model, *J. Mod. Opt.* **40**, 1195 (1993).
- [11] P. Knight and P. Milonni, The Rabi frequency in optical spectra, *Phys. Rep.* **66**, 21 (1980).
- [12] P. Grangier, G. Roger, A. Aspect, A. Heidmann, and S. Reynaud, Observation of photon antibunching in phase-matched multiatom resonance fluorescence, *Phys. Rev. Lett.* **57**, 687 (1986).
- [13] A. S. Prasad, J. Hinney, S. Mahmoodian, K. Hammerer, S. Rind, P. Schneeweiss, A. S. Sørensen, J. Volz, and A. Rauschenbeutel, Correlating photons using the collective nonlinear response of atoms weakly coupled to an optical mode, *Nat. Photon.* **14**, 719 (2020).
- [14] G. Maret and P. E. Wolf, Multiple light scattering from disordered media. The effect of Brownian motion of scatterers, *Z. Phys. B* **65**, 409 (1987).
- [15] D. J. Pine, D. A. Weitz, P. M. Chaikin, and E. Herbolzheimer, Diffusing wave spectroscopy, *Phys. Rev. Lett.* **60**, 1134 (1988).
- [16] D. A. Weitz, D. J. Pine, P. N. Pusey, and R. J. A. Tough, Nondiffusive Brownian motion studied by diffusing-wave spectroscopy, *Phys. Rev. Lett.* **63**, 1747 (1989).
- [17] S. Fraden and G. Maret, Multiple light scattering from concentrated, interacting suspensions, *Phys. Rev. Lett.* **65**, 512 (1990).
- [18] P. Hébraud, F. Lequeux, J. P. Munch, and D. J. Pine, Yielding and rearrangements in disordered emulsions, *Phys. Rev. Lett.* **78**, 4657 (1997).
- [19] T. Durduran, G. Yu, M. G. Burnett, J. A. Detre, J. H. Greenberg, J. Wang, C. Zhou, and A. G. Yodh, Diffuse optical measurement of blood flow, blood oxygenation, and metabolism in a human brain during sensorimotor cortex activation, *Opt. Lett.* **29**, 1766 (2004).
- [20] A. Eloy, Z. Yao, R. Bachelard, W. Guerin, M. Fouché, and R. Kaiser, Diffusing-wave spectroscopy of cold atoms in ballistic motion, *Phys. Rev. A* **97**, 013810 (2018).
- [21] B. R. Mollow, Power spectrum of light scattered by two-level systems, *Phys. Rev.* **188**, 1969 (1969).
- [22] P. W. Milonni, Why spontaneous emission? *Am. J. Phys.* **52**, 340 (1984).
- [23] L. Ortiz-Gutiérrez, R. C. Teixeira, A. Eloy, D. Ferreira, R. Kaiser, R. Bachelard, and M. Fouché, Mollow triplet in cold atoms, *New J. Phys.* **21**, 093019 (2019).
- [24] D. Ferreira, R. Bachelard, W. Guerin, R. Kaiser, and M. Fouché, Connecting field and intensity correlations: The Siegert relation and how to test it, *Am. J. Phys.* **88**, 831 (2020).
- [25] R. Loudon, *The Quantum Theory of Light* (Oxford Science Publications, New York, 1973).
- [26] B. L. Ng, C. H. Chow, and C. Kurtsiefer, Observation of the Mollow triplet from an optically confined single atom, *Phys. Rev. A* **106**, 063719 (2022).
- [27] R. J. Glauber, The quantum theory of optical coherence, *Phys. Rev.* **130**, 2529 (1963).
- [28] C. Skornia, J. von Zanthier, G. S. Agarwal, E. Werner, and H. Walther, Nonclassical interference effects in the radiation from coherently driven uncorrelated atoms, *Phys. Rev. A* **64**, 063801 (2001).
- [29] S. Wolf, S. Richter, J. von Zanthier, and F. Schmidt-Kaler, Light of two atoms in free space: Bunching or antibunching? *Phys. Rev. Lett.* **124**, 063603 (2020).
- [30] A. A. Svidzinsky, J.-T. Chang, and M. O. Scully, Cooperative spontaneous emission of  $n$  atoms: Many-body eigenstates, the effect of virtual lamb shift processes, and analogy with radiation of  $n$  classical oscillators, *Phys. Rev. A* **81**, 053821 (2010).
- [31] F. Cottier, R. Kaiser, and R. Bachelard, Role of disorder in super- and subradiance of cold atomic clouds, *Phys. Rev. A* **98**, 013622 (2018).
- [32] J. Johansson, P. Nation, and F. Nori, QuTiP 2: A Python framework for the dynamics of open quantum systems, *Comput. Phys. Commun.* **184**, 1234 (2013).
- [33] K. Mølmer, Y. Castin, and J. Dalibard, Monte Carlo wavefunction method in quantum optics, *J. Opt. Soc. Am. B* **10**, 524 (1993).
- [34] J. W. Noh, A. Fougères, and L. Mandel, Operational approach to the phase of a quantum field, *Phys. Rev. A* **45**, 424 (1992).
- [35] J. R. Torgerson and L. Mandel, Is there a unique operator for the phase difference of two quantum fields? *Phys. Rev. Lett.* **76**, 3939 (1996).
- [36] A. J. F. Siegert, *On the Fluctuations in Signals Returned by Many Independently Moving Scatterers*, Report No. 465 (Radiation Laboratory, Massachusetts Institute of Technology, 1943).
- [37] R. H. Dicke, Coherence in spontaneous radiation processes, *Phys. Rev.* **93**, 99 (1954).
- [38] K. Baumann, C. Guerlin, F. Brennecke, and T. Esslinger, Dicke quantum phase transition with a superfluid gas in an optical cavity, *Nature (London)* **464**, 1301 (2010).

- [39] V. M. Bastidas, C. Emary, B. Regler, and T. Brandes, Nonequilibrium quantum phase transitions in the Dicke model, *Phys. Rev. Lett.* **108**, 043003 (2012).
- [40] G. Ferioli, A. Glicenstein, I. Ferrier-Barbut, and A. Browaeys, Observation of a non-equilibrium superradiant phase transition in free space, *Nat. Phys.* **19**, 1345 (2023).
- [41] M. O. Araújo, L. S. Marinho, and D. Felinto, Observation of nonclassical correlations in biphotons generated from an ensemble of pure two-level atoms, *Phys. Rev. Lett.* **128**, 083601 (2022).
- [42] D. Meiser and M. J. Holland, Intensity fluctuations in steady-state superradiance, *Phys. Rev. A* **81**, 063827 (2010).